the DC-link voltage, and the q-axis current can be used to regulate the reactive power, which can be seen in Fig.3.

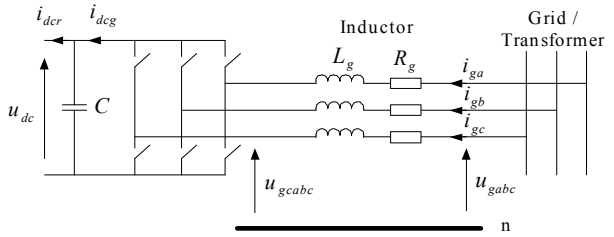

Fig.3 Schematic diagram of a grid-side converter connected to the grid/transformer

Fig.3 shows the schematic diagram of the grid-side PWM voltage source converter, where u_{gabc} are the three-phase grid voltages, u_{gcabc} are the three-phase grid-side converter voltages, i_{ga}, i_{gb}, i_{gc} are the three-phase grid-side converter currents, R_g and L_g are the inductor resistance and inductance, i_{dcg}, i_{dcr} are the grid-side and rotor-side DC currents, C is the DC-link capacitor.

The voltage balance equation of the grid-side converter can be expressed as:

$$\begin{bmatrix} u_{ga} \\ u_{gb} \\ u_{gc} \end{bmatrix} = R_g \begin{bmatrix} i_{ga} \\ i_{gb} \\ i_{gc} \end{bmatrix} + L_g \frac{d}{dt} \begin{bmatrix} i_{ga} \\ i_{gb} \\ i_{gc} \end{bmatrix} + \begin{bmatrix} u_{gca} \\ u_{gcb} \\ u_{gcc} \end{bmatrix} \tag{3}$$

By using the abc-to-dq transformation matrix, the following equation can be given:

$$\begin{cases} u_{gd} = R_g i_{gd} + L_g \dfrac{di_{gd}}{dt} - \omega_e L_g i_{gq} + u_{\mathrm{gcd}} \\ u_{gq} = R_g i_{gq} + L_g \dfrac{di_{gq}}{dt} + \omega_e L_g i_{gd} + u_{gcq} \end{cases} \tag{4}$$

where u_{gd}, u_{gq} are the grid voltages in d-and q-axis, u_{gcd}, u_{gcq} are the grid-side converter voltages in d- and q-axis, i_{gd}, i_{gq} are the grid-side converter currents in d-and q-axis, ω_e is the electrical angular velocity of the grid voltage.

Neglecting the switch losses of the converter, the following equations can be obtained [16,18].

$$\begin{cases} u_{dc} i_{dcg} = \dfrac{3}{2} u_{gd} i_{gd} \\ u_{gd} = \dfrac{m}{2} u_{dc} \\ i_{dcg} = \dfrac{3}{4} m i_{gd} \\ C \dfrac{du_{dc}}{dt} = i_{dcg} - i_{dcr} \end{cases} \tag{5}$$

where m is the PWM modulation depth of the grid-side converter.

From the above equations, it can be seen that the currents i_{gd} and i_{gq} can be regulated by using u_{gcd} and u_{gcq} respectively. The control scheme utilises current control loops by i_{gd} and i_{gq}, the i_{gd} reference value can be derived from the DC-link voltage error. In addition, the i_{gq} reference determines the reactive power flow between the grid and the grid-side converter. Usually the i_{gq} reference value can be set to zero, which ensures zero reactive power exchange between the grid and the grid-side converter.

A vector-control scheme for the grid-side PWM voltage source converter is shown in Fig.4, where u^*_{gcabc} represents the reference values of the three-phase grid-side converter voltages, $u^*_{\mathrm{gcd}}, u^*_{gcq}$ are the reference values of the grid-side converter voltages

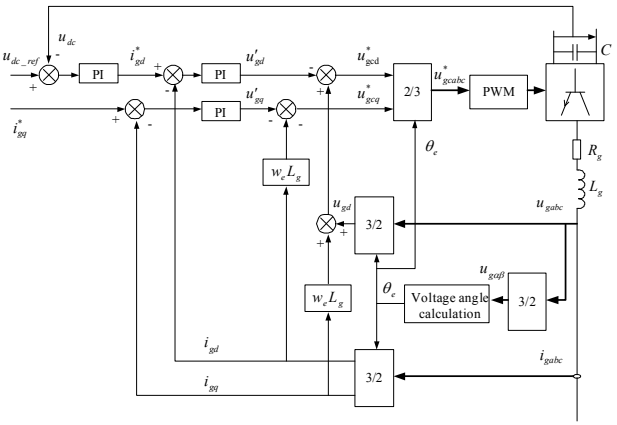

Fig. 4 Scheme of grid-side PWM converter control

in d-and q-axis, i^*_{gd}, i^*_{gq} are the reference values of the grid-side converter currents in d-and q-axis.

2.3 Control Strategy of Rotor-side Converter

In order to analyze the transient performances of a wind turbine generator, a mathematical model including electromagnetic transients both in the stator and the rotor circuits of DFIG is usually used. According to a standard per-unit notation in a reference frame rotating at synchronous speed and a motor convention, the transient models of a grid-connected DFIG can be represented by the detailed differential equations of the flux linkages [11,12]

$$\begin{cases} u_{sd} = R_s i_{sd} + \dfrac{d\psi_{sd}}{dt} - \omega_s \psi_{sq} \\ u_{sq} = R_s i_{sq} + \dfrac{d\psi_{sq}}{dt} + \omega_s \psi_{sd} \\ u_{rd} = R_r i_{rd} + \dfrac{d\psi_{rd}}{dt} - s\omega_s \psi_{rq} \\ u_{rq} = R_r i_{rq} + \dfrac{d\psi_{rq}}{dt} + s\omega_s \psi_{rd} \end{cases} \tag{6}$$

The equations of flux linkage can be given as：

$$\begin{cases} \psi_{sd} = L_s i_{sd} + L_m i_{rd} \\ \psi_{sq} = L_s i_{sq} + L_m i_{rq} \\ \psi_{rd} = L_r i_{rd} + L_m i_{sd} \\ \psi_{rq} = L_r i_{rq} + L_m i_{sq} \end{cases} \tag{7}$$

Where ω_s is the synchronous speed；u, ψ, i, R, L are the voltage, flux linkage, current, resistance and inductance；L_m is the mutual inductance between rotor and stator；subscript s, r indicate the stator and rotor of electric machine, respectively; subscript d, q indicate the d, q components, respectively; s is slip ratio of DFIG.

The stator active and reactive power of a DFIG can be given as:

$$\begin{cases} P_s = \dfrac{3}{2}\left(u_{sd} i_{sd} + u_{sq} i_{sq}\right) \\ Q_s = \dfrac{3}{2}\left(u_{sq} i_{sd} - u_{sd} i_{sq}\right) \end{cases} \tag{8}$$

In order to implement the active and reactive power decoupling control, the stator voltage can be oriented, that is $u_{sd}=U_s$, $u_{sq}=0$.

The stator active and reactive power can be further obtained as

$$\begin{cases} P_s = -\dfrac{3 L_m U_s i_{rd}}{2 L_s} \\ Q_s = \dfrac{3}{2}\left(\dfrac{U_s^2}{\omega_s L_s} + \dfrac{U_s L_m i_{rq}}{L_s}\right) \end{cases} \tag{9}$$

The electromagnetic torque of a DFIG can be also given as：

$$T_e = -n_p \frac{L_m}{L_s} \vec{\psi}_s \times \vec{i}_r = -n_p \frac{L_m}{L_s} \psi_s i_{rd} \tag{10}$$

Fig.5 shows a vector-control scheme for the rotor-side PWM voltage source converter, where u^*_{abcr} represents the reference values of the three-phase rotor voltages, u^*_{rd}, u^*_{rq} are the reference values of the rotor voltages in d-and q-axis, i^*_{rd}, i^*_{rq} are the reference values of the rotor currents in d-and q-axis. The stator active and reactive power can be controlled by regulating the d-, q-axis components of the rotor current. The compensated voltage equations can be shown as [12]

$$\begin{cases} \Delta u_{rd} = R_r i_{rd} - s\omega_s (L_r i_{rq} + L_m i_{sq}) \\ \Delta u_{rq} = R_r i_{rq} + s\omega_s (L_r i_{rd} + L_m i_{sd}) \end{cases} \tag{11}$$

3 Transient Simulation of Doubly Fed Wind Turbine with Different Models

Fig.6 shows the schematic diagram of a doubly fed wind turbine connected to the grid. In the following simulation, the input mechanical torque from wind energy can be kept at constant value during a grid voltage drop, which means the pitch control system can not be in action during the electrical transient. In addition, the rotor-side converter is assumed to ride through the fault current even though for a thee-phase short-circuit fault at the stator terminals of DFIG. The main parameters of a 3MW doubly fed wind turbine system are shown in Table 1.

In order to show and compare the effects of the different drive-train models on the transient performances, the transient performances are simulated for the doubly fed wind turbine with different grid voltage drops and different initial generator speeds. The following cases are investigated for 40% and 80% grid voltage drops under a super-synchronous and sub-synchronous generator speed, respectively.

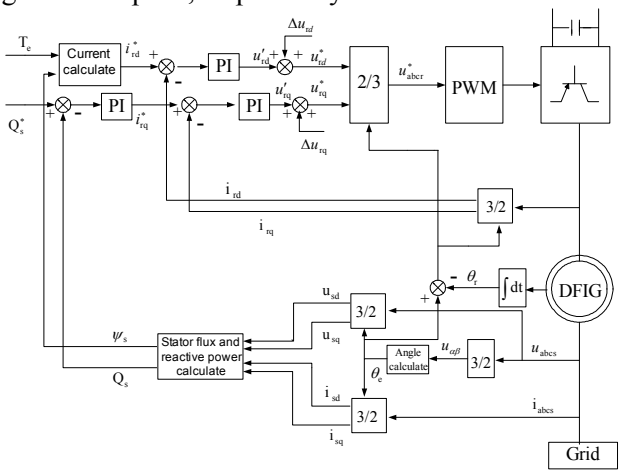

Fig. 5 Block diagram of active and reactive power decoupling control for the rotor-side converter

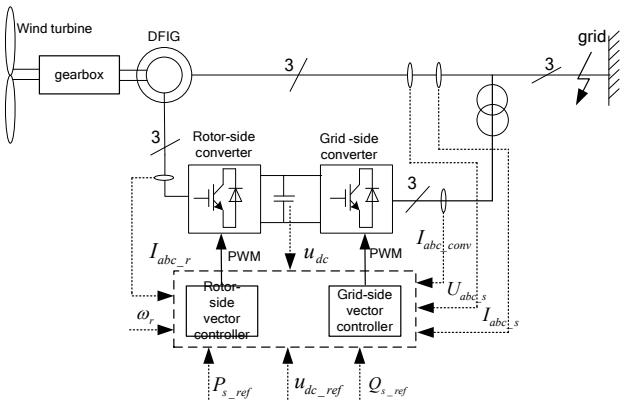

Fig.6 Control diagram of a grid connected doubly fed wind turbine

Table 1 Main parameters of a 3MW doubly fed wind turbine system

Main parameters	Value
Wind turbine	
Per unit inertia constant of hub H_w (s)	4.54
Torsional stiffness of low-speed shaft K_s (p.u./el.rad)	0.3
DFIG	
Normal power base (MW)	3
Voltage base U_N(V)	690
Stator resistance R_s (p.u.)	0.0071
Rotor resistance R_r (p.u.)	0.005
Stator leakage inductance $X_{s\sigma}$ (p.u.)	0.171
Rotor leakage inductance $X_{r\sigma}$ (p.u.)	0.1791
Mutual inductance X_m (p.u.)	2.9
Per unit inertia constant of generator H_g (s)	0.5

3.1 40% Voltage Dip under Super-synchronous Operation

In this case, the symmetrical three-phase stator voltage drops 40% at t=0.05s, and at t=0.15s the voltage is restored to its pre-sag value. Before the grid fault occurs, the generator rotor speed is set to be 1.2 p.u..

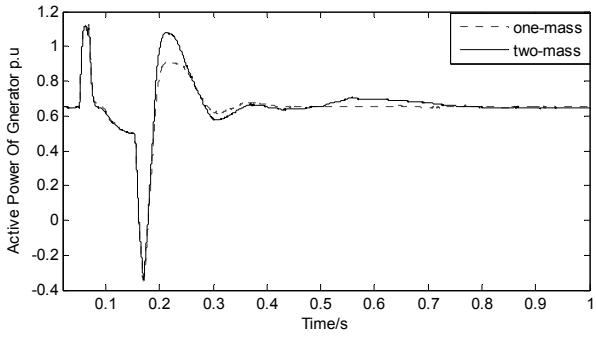

(a) Active power of generator

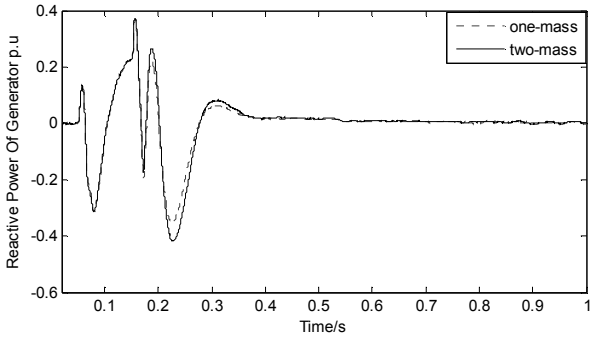

(b) Reactive power of generator

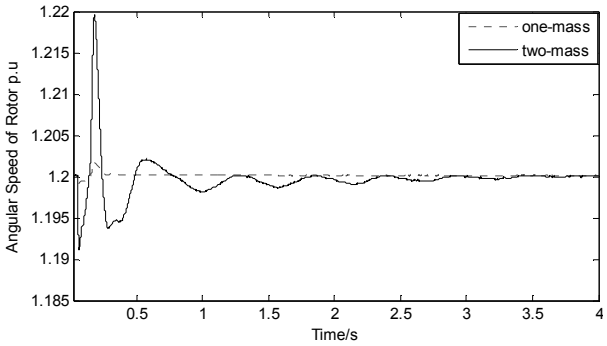

(c) Angular speed of rotor

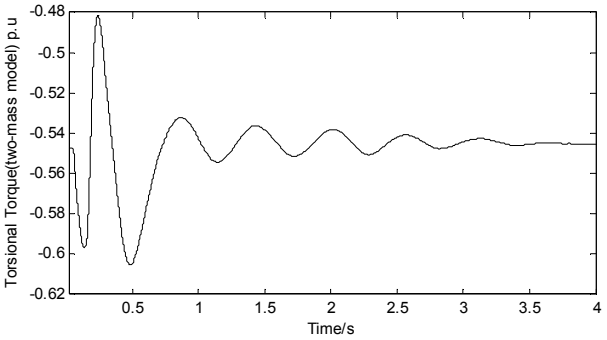

(d) Torsional torque

Fig. 7 Transient responses of 40% voltage drop under the super-synchronous operation

Fig.7 shows the transient behaviors under this case. As it can be seen from Fig.7(a) that the active power has a larger oscillation during the post-fault with the two-mass model in comparison with one-mass model of the wind turbine drive train. The results have shown that the maximal active power reaches about 1.1p.u. using the two-mass model when the grid voltage fault is cleared, however, this value is only 0.85p.u. by using the one-mass model. In addition, the reactive power is rarely affected by using different drive train models. As it can be seen from Fig.7(c) that the rotor speed of DFIG has a larger oscillation during the post-fault for the two-mass model in comparison with the one-mass model. The maximal angular speed can reach about 1.219p.u. considering a two-mass model when the grid voltage fault is cleared, however, this value is only 1.203p.u. with the one-mass model. The angular speed keeps oscillating until t=3.5s by using the two-mass model, however, at t=0.25s the angular speed keeps its pre-sag value by using the one-mass model. Furthermore, it can be also seen that the torsional torque has a large oscillation by using a two-mass model.

3.2 40% Voltage Dip under Sub-synchronous Operation

In this case, the symmetrical three-phase stator voltage drops 40% at t=0.05s, and at t=0.15s the voltage is restored to its pre-sag value. Before the grid fault occurs, the generator rotor speed is set to be 0.87 p.u..

As it can be seen from Fig.8(a) and Fig.8(b), the active power and reactive power are rarely affected by using different drive train models. In addition, as it can be also seen from Fig.8(c) and Fig.8(d), the angular speed of rotor and the torsional torque have a larger oscillation during the post-fault by using the two-mass model in comparison with a one-mass model. The results have shown the angular speed and the torsional torque keep oscillating until t=11s by using the two-mass model when the grid voltage fault is cleared, however, at t=0.25s the angular speed keeps its pre-sag value by using the one-mass model.

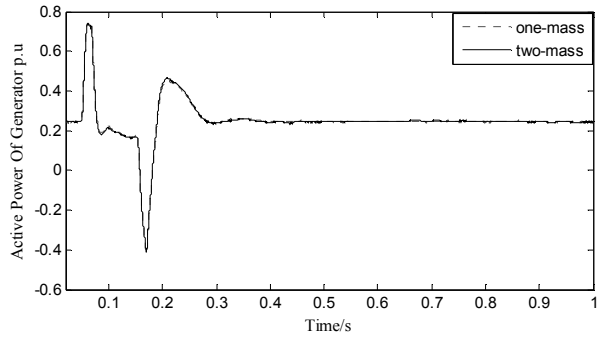

(a) Active power of generator

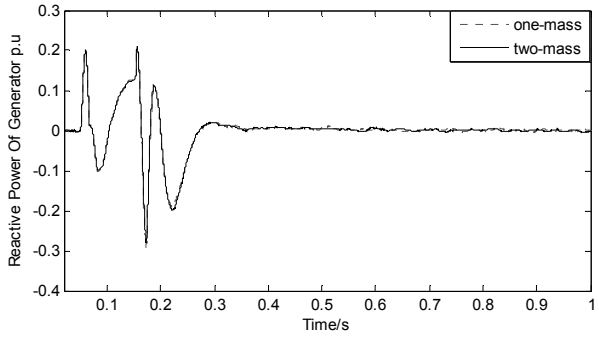

(b) Reactive power of generator

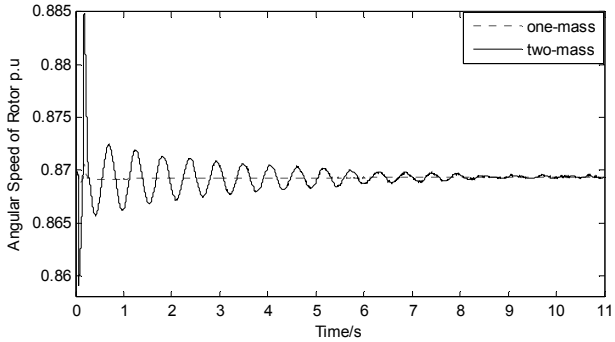

(c) Angular speed of rotor

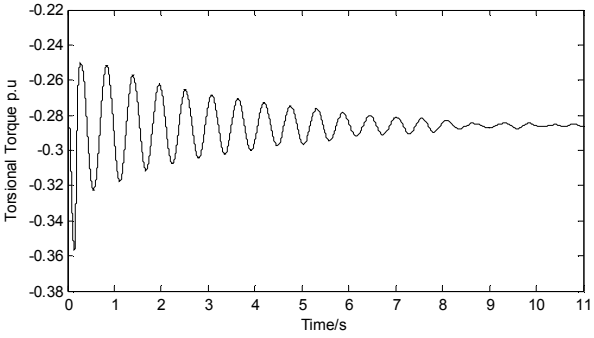

(d) Torsional torque

Fig. 8 Transient responses of 40% voltage drop under the sub-synchronous operation

3.3 80% Voltage Dip under Super-synchronous Operation

In this case, the symmetrical three-phase stator voltage drops 80% at t=0.05s, and at t=0.15s the voltage is restored to its pre-sag value. Before the grid fault occurs, the generator rotor speed is set to be 1.2 p.u..

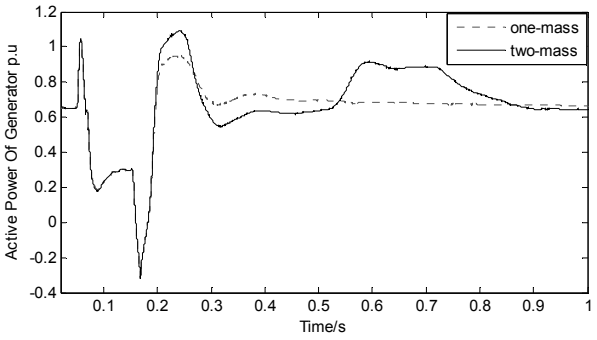

(a) Active power of generator

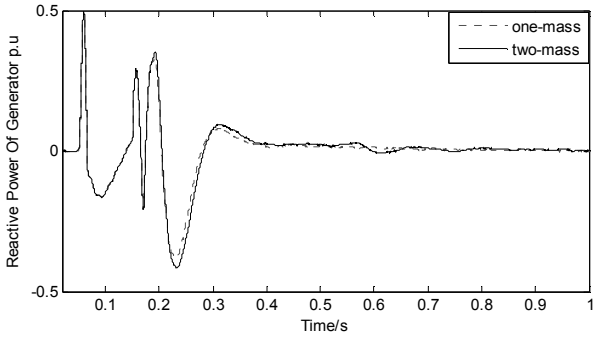

(b) Reactive power of generator

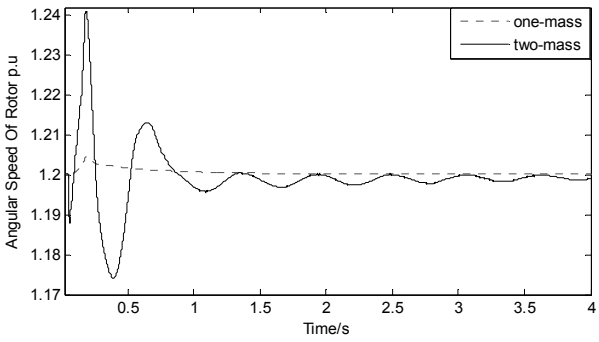

(c) Angular speed of rotor

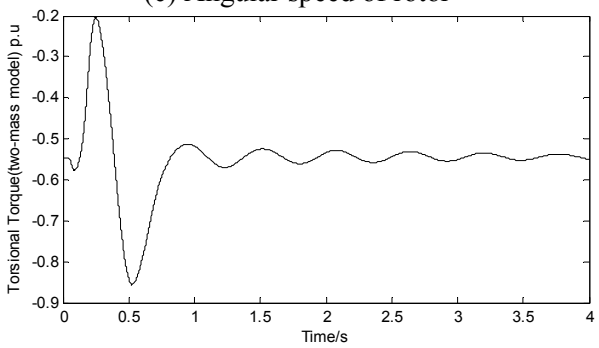

(d) Torsional torque

Fig.9 Transient responses of 80% voltage drop under the super-synchronous operation

As it can be seen from Fig.9(a), the active power has a larger oscillation during the post-fault by using the two-mass model in comparison with a one-mass model. The results have shown that the maximal active power can reach about 1.1p.u. by using a two-mass model when the grid voltage fault is cleared, however, this value is only 0.85p.u. by using one-mass model. The second peak value of the active power is 0.915p.u. by using a two-mass model during the post-fault, however, this value is only 0.707p.u. for the case voltage drops 40% in Fig.7(a). As it can be also seen from Fig.9(c) that the maximal angular speed can reach about 1.24p.u. by using a two-mass model when the grid voltage fault is cleared, which is larger than the value of the case voltage drops 40%. In addition, at t=3.5s the rotor speed can not be kept steady. Furthermore, as it can be seen in Fig.9(d) that the maximal torsional torque is -0.2p.u., this value is -0.48p.u. for the case voltage drops 40% Fig.7(d).

Therefore, it can be seen from the above several comparisons that it is necessary to use a two-mass drive train model for correctly analyzing the transient performance of the doubly fed wind turbine. The level of grid voltage drop, and different initial rotor speed condition have an important impact on the transient performances of the doubly fed wind turbine, especially for the higher level of grid voltage drop and the super-synchronous speed condition.

4 Transient Responses of Doubly Fed Wind Turbine with Different Parameters

In order to further analyze the effects of the wind turbine drive train shaft flexibility on the transient performance of the doubly fed wind turbine, based on the presented two-mass model of the wind turbine drive train, the transient responses are investigated with different shaft flexibility and inertia constant of turbine and generator. In the following simulation, the grid fault condition is assumed to be the same as 3.3.

Case-I: *Simulation on different shaft flexibilities*

The objective of this case is to present the effect of the shaft stiffness on the transient performances of the doubly fed wind turbine. Simulation is performed by using 3 values of 10, 5 and 0.3 for shaft stiffness constant, respectively. The transient responses of the active power and the rotor speed with different shaft flexibilities are shown in Fig. 10.

As it can be seen that the transient behaviors are closely dependent on the shaft stiffness constant by using the two-mass model. The active power and the angular speed response occur much higher oscillation amplitude and lower oscillation frequency when the smaller K_s value is used, it also need longer time to restore steady state after the grid fault is cleared. Thus, the results have shown that: as the stiffness constant decreases, the torsion frequency becomes lower and the shaft flexibility becomes larger, the influence of the shaft stiffness on transient performances of the doubly fed wind turbine becomes more and more obvious.

Case-II: *Simulation on different inertia constants*

The objective of this case is to present the effect of different inertia constants on the transient performances of the doubly fed wind turbine. Assumed the shaft stiffness is a constant, viz., K_s =0.3, the flowing simulation is performed by using 4 values for total inertia constants and 3 different H_w/H_g values of the WTGS, respectively. The responses of the rotor speed are shown as Fig.11(a)-(b).

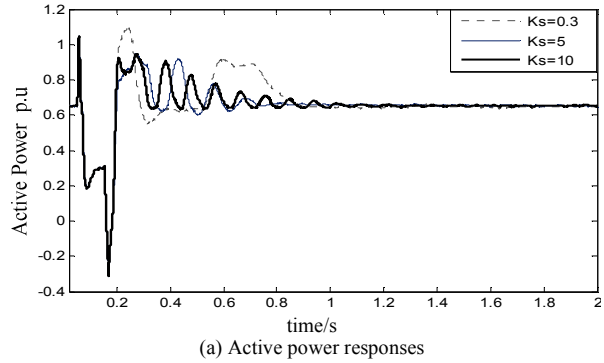

(a) Active power responses

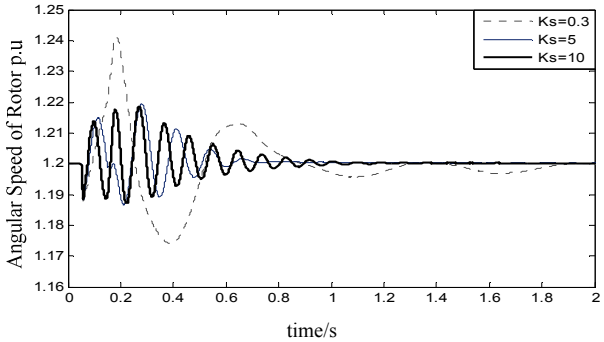

(b) Rotor Angular speed responses

Fig. 10 Transient responses of a doubly fed wind turbine with different stiffness constants

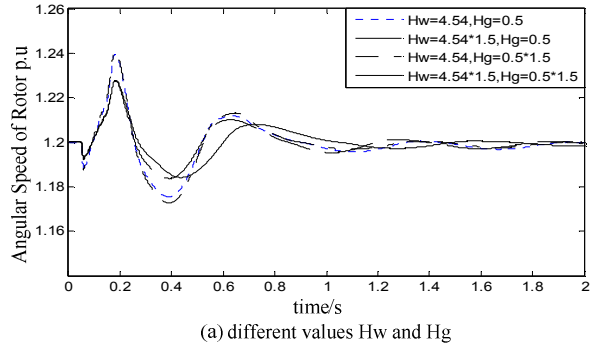

(a) different values Hw and Hg

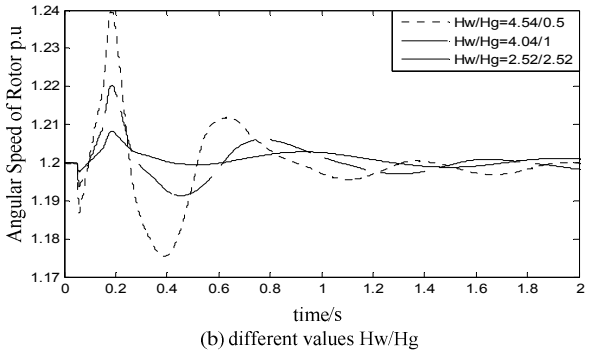

(b) different values Hw/Hg

Fig. 11 Transient responses of a doubly fed wind turbine with different inertia constants

As it can be seen that the transient performances are also closely correlated to the inertia constant of the wind turbine and the generator. Either H_w or H_g is increased by 50%, the oscillation amplitude of the rotor speed can be decreased, however, the oscillation amplitude can be more significantly decreased with the 50% increase of H_g as compared with the 50% increase of H_w. When both the H_w and H_g are increased by 50%, the rotor speed oscillation can be reduced obviously. In addition, assumed the total inertia of the WTGS is a constant, viz., (H_w+H_g)=4.54s, it can be also seen that the transient performances are dependent on the inertia constant ratio of the wind turbine and the generator H_w/H_g, it can be concluded that with the increase of the inertia constant ratio, the oscillation amplitude of the rotor speed can be also increased obviously.

5 Transient Responses of Doubly fed Wind Turbine with an Active Crowbar

In order to show the effects of the active crowbar on the transient performances of the doubly fed wind turbine, the transient performances are investigated with different trip time of the active crowbar circuit. Fig. 12 shows a schematic of a crowbar protection with three-phase AC switch and bypass resistor.

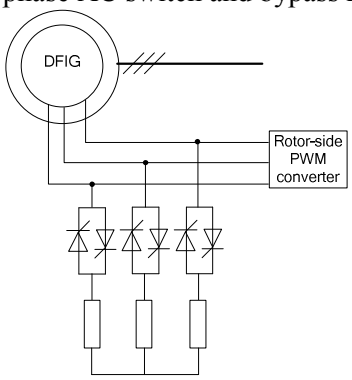

Fig. 12 Schematic diagram of a crowbar protect circuit with three-phase AC switch and bypass resistor

Case-I: In this case, the transient responses of the doubly fed wind turbine under 80% voltage drop are simulated by using the presented two-mass model. Before the grid fault occurs, the generator rotor speed is set to be 1.2p.u.. The symmetrical three-phase stator voltage drops 80% at t=0.2s, and at t=0.35s the voltage is restored to its pre-sag value. The crowbar circuit switches in when the grid fault is occurred, and simultaneously the rotor-side converter is closed and the grid-side converter is also in operation. After the grid fault is cleared, the crowbar circuit switch out and the rotor-side converter restart to work. The transient

performances of the doubly fed wind turbine with the active crowbar are shown in Fig. 13.

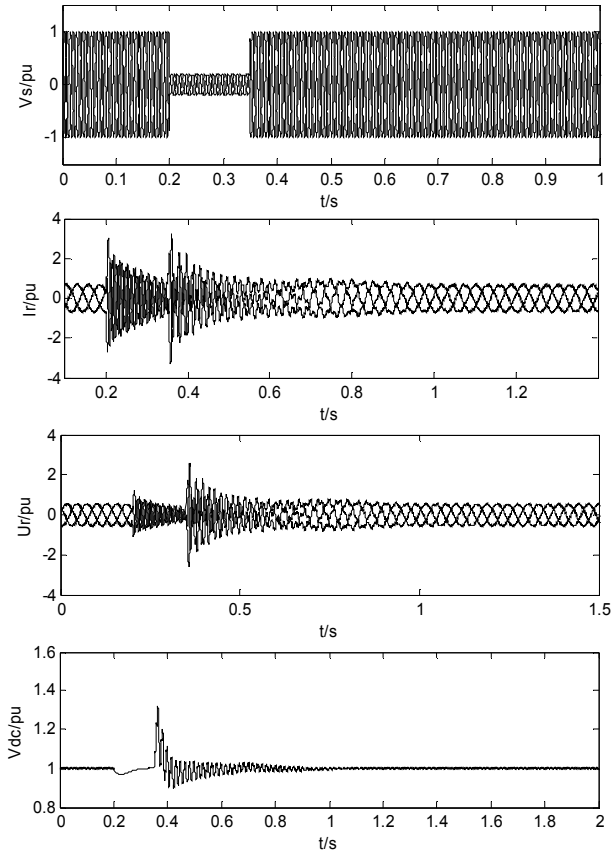

Fig. 13 Transient responses when the stator voltage drops 80% and the crowbar circuit trips at 0.35s

As it can be seen from Fig.13 that when the crowbar circuit is tripped at 0.35s, the rotor current is 3.7p.u. which exceeds the threshold value, and the rotor voltage also exceeds the threshold value after the grid fault is cleared. The maximum value of dc-link voltage is about 1.32p.u..

Case-II: In this case, the transient responses of the doubly fed wind turbine under 80% voltage drops are also simulated. But the active crowbar circuit trips at t=0.5s, that is to say, the crowbar circuit will continue to work for 0.15s after the gird fault is cleared. The transient performances of the doubly fed wind turbine with the active crowbar are shown in Fig. 14.

As it can be seen from Fig.14 that when the crowbar circuit trips at 0.5s, the dc capacitor voltages, the rotor current do not exceed the threshold value. Furthermore, the results have shown that there is much smaller oscillation of the transient performances as compared with the case I. Thus, it is necessary to select the appropriate trip time of the crowbar circuit to reduce the oscillation and improve the transient stability of the doubly fed wind turbine.

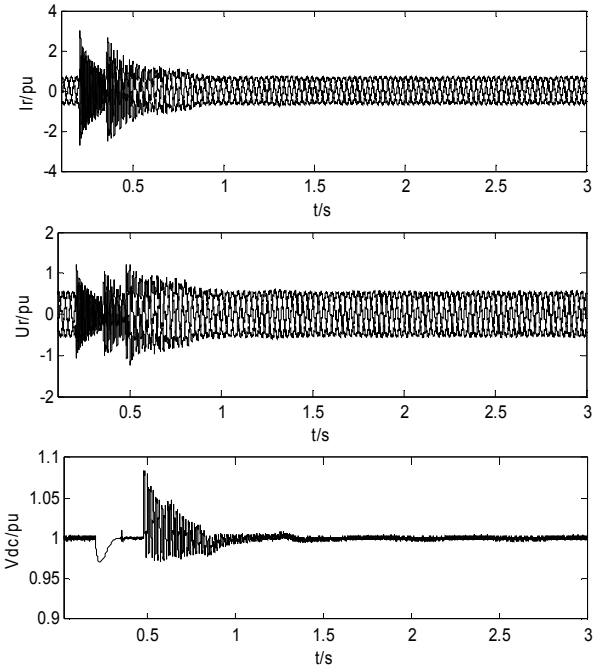

Fig. 14 Transient responses when the stator voltage drops 80% and the crowbar circuit trips at 0.5s

6 Conclusions

In order to investigate the transient performances of a doubly fed wind turbine with the appropriate transient models, a one-mass lumped model and a two-mass shaft flexible model of the wind turbine drive train system are presented. Based on the control strategies of the grid-side converter and the rotor-side converter of DFIG, the transient behaviors are simulated and compared by using different drive train models, under the conditions of different voltage sags and different generator initial speed. The simulation results have shown the wind turbines system model incorporating a two-mass drive train shaft model is important to analyze exactly the transient performance of the doubly fed wind turbine, the level of grid voltage drop and different initial rotor speed condition have an important impact on the transient performances of the doubly fed wind turbine, especially for the higher level of grid voltage drop and the super-synchronous speed condition. In accordance to the two-mass model with the more flexibility of the drive train, with the decrease of the total inertia constant or with the increase of the inertia constant ratio, the transient performances may cause larger oscillation, and maybe result into the unstable

operation of WTGS. Furthermore, the trip time of the active crowbar circuit also has an important influence on the transient behaviors, after the grid fault is cleared, the crowbar circuit continues to work a long time, which can be helpful to improve the low voltage ride-through ability. The results of the investigation of the transient models and the transient performances of the doubly fed wind turbine will provide a good technical support to the transient impacts of the integration of wind farms into utilities network in the future.

Acknowledgment
This research work is supported by both Natural Science Foundation of China (NSFC) under Grant No.50607022 and Scientific Research Foundation of State Key Laboratory of Power Transmission Equipment & System Security and New Technology under Grant No. 2007DA10512710101, also supported by the Fundamental Research Funds for the Central Universities (CDJXS10151152). The authors are grateful for their financial support.

References:
[1] Z. Chen, F. Blaabjerg, Wind farm—a power source in future power systems, *Renewable & Sustainable Energy Reviews*, Vol.13, No.6-7, 2009, pp. 1288-1300.
[2] Jingjing Zhao, Xin Li, Jutao Hao, Voltage Control Scheme in Distribution Network with Double Feed Induction Generator Wind Farm, *WSEAS Transactions on Circuits and Systems*, Vol.8, No.8, 2009, pp. 709-718.
[3] Wu Dingguo, Wang Zhixin, Modeling and design of control system for variable speed wind turbine in all operating region, *WSEAS Transactions on Circuits and Systems*, Vol.7, No.5, 2008, pp. 438-443.
[4] Hengameh Kojooyan Jafari, Simulation of doubly-fed machine with improved wind turbine, *WSEAS Transactions on Circuits and Systems*, Vol.8, No.2, 2009, pp. 217-226.
[5] Li Dong, Chen Chen, A study on dynamic model of wind turbine generator sets, *Proc. of CSEE*, Vol.25, No.3, 2005, pp. 115-119.
[6] Yin Ming, Li Gengyin, Zhou Ming, Zhao Chengyong, Analysis and comparison of dynamic models for the doubly fed induction generator wind turbine, *Automation of Electric Power Systems*, Vol.30, No.13, 2006, pp. 22-27.
[7] S.Seman, F.Iov , J.Niiranen , A.Arkkio, Advanced modeling of doubly fed induction generator wind turbine under network disturbance, in *Proc. of 5th Int. Workshop on Large-scale Integration of Wind Power and Transmission Networks for offshore Wind Farms*, Glasgow, U.K, Apr.7-8, 2005, pp. 305-314.
[8] Liu Qihui, He Yikang, Zhang Janhua, Operation control and modeling simulation of ac-excited variable-speed constant-frequency (AVESCF) wind power generator, *Proc. of CSEE*, Vol.26, No.5, 2006, pp. 43-50.
[9] Jesus Lopez, Pablo Sanchis, Xavier Roboam, Luis Marroyo, Dynamic behavior of the doubly fed induction generator during three phase voltage dip, *IEEE Trans Energy Convers* ,Vol.22, No.3, 2007, pp. 707-717.
[10] T. Petru, T. Thiringer, Modeling of wind turbines for power system studies, *IEEE Trans Power Syst*, Vol.17, No.4, 2002, pp.1132-1139.
[11] SK. Salman, J. T. Anitul, Windmill modeling consideration and factors influencing the stability of a grid-connected wind power-based embedded generator, *IEEE Trans Power Syst*, Vol.18, No.2, 2003, pp. 793-802.
[12] Chen Shuyong, Dai Huizhu, Bai Xiaomin, Reliability model of wind power plants and its application, *Proc. of CSEE*, Vol.20, No.3, 2000, pp. 26-29.
[13] Tao Sun, Z. Chen, F Blaabjerg, Transient analysis of grid-connected wind turbines with DFIG after an external short-circuit fault, in *Nordic Wind Power Conference*, 1-2. March, 2004, pp. 1-7.
[14] Tao Sun, Z. Chen, F. Blaabjerg, Transient stability of DFIG wind turbines at an external short-circuit fault, *Wind Energy*, Vol.8, No.3, 2005, pp. 345-360.
[15] J.B.Ekanayake, L.Holdsworth, X.G.Wu, N.Jenkins, Dynamic modeling of doubly fed induction generator wind turbines, *IEEE Trans Power Syst*, Vol.18, No.2, 2003, pp. 803-809.
[16] Li Hui, Yang Shunchang, Liao Yong, Studies on excitation control of power system voltage oriented for doubly fed generators connected to an infinite bus, *Proc. of CSEE*, Vol.23, No.8, 2003, pp. 159-162.
[17] Daniel J. Trudnowski, Jawad M. Khan, Eric M. Petritz, Fixed-speed wind generator and wind park modeling for transient stability studies, *IEEE Trans Power Syst*, Vol.19, No.4, 2004, pp. 1911-1917.
[18] R.Pena, J. C. Clare, G. M. Asher, Doubly fed induction generator using back-to-back pwm converters and its application to variable-speed wind-energy generation, *IEE Proc-Electr Power Appl*, Vol.143, No.3, 1996, pp. 231-241.